Materials Reports Solidwaste & Ecomaterials

Materials Reports: Solidwaste and Ecomaterials

Journal Homepage: www.sciopen.com/journal/3078-4093

Original Research Report

Effects of CO_2 curing on hydration behavior, strength development, and microstructural evolution of coal gangue-based cementitious materials

Xuyang Zang [1], Lei Zhang [1, 2, *], Dehui Zhu [1], Zhijun Li [3], Tao Li [4], Yitong Ren [5], Moncef L. Nehdi [6, *]

[1] School of Civil and Transportation Engineering, Hebei University of Technology, Tianjin 300041, China

[2] Key Laboratory of Xinjiang Coal Resources Green Mining, Ministry of Education, Xinjiang Institute of Engineering, Urumqi 830023, China

[3] School of Resources and Civil Engineering, Northeastern University, Shenyang 110819, China

[4] Inner Mongolia Long'an Safety Assessment Co., Ltd, Baotou 014000, China

[5] Department of Water Resources Engineering, Hebei University of Water Resources and Electric Engineering, Cangzhou 061001, China

[6] College of Engineering, University of Guelph, 50 Stone Road East, Guelph, ON N1G 2W1, Canada

Abstract: The large-scale generation of coal gangue in China presents urgent challenges for resource utilization and carbon emission reduction. This study investigates the preparation and performance optimization of a limestone–calcined coal gangue cement (LCC) system under CO_2 mineralization curing. Experimental methods—including X-ray diffraction (XRD) and mercury intrusion porosimetry (MIP)—combined with molecular dynamics (MD) simulations were employed to examine how $Ca(OH)_2$ content and pore structure influence hydration, carbonation, and strength development. Results showed that moderate incorporation of $Ca(OH)_2$ (10–20 wt% relative to gangue) under CO_2 curing enhanced 28-day compressive strength by up to 14.9%, owing to the formation of $CaCO_3$ which densifies the matrix and reduces porosity. However, excessive $Ca(OH)_2$ caused micropores and strength loss. MIP revealed that refined pore structure, particularly increased gel pores (< 10 nm), was correlated with strength gains. MD simulations further demonstrated that larger pore sizes (e.g., 24 Å) promoted CO_2 diffusion and adsorption, while nanoscale confinement hindered transport due to structured water layers. Overall, the LCC system with optimized $Ca(OH)_2$ content and pore architecture not only matches the strength of ordinary Portland cement but also enables CO_2 sequestration. This research offers a low-carbon strategy for coal gangue valorization and provides multiscale insights for designing sustainable cementitious materials.

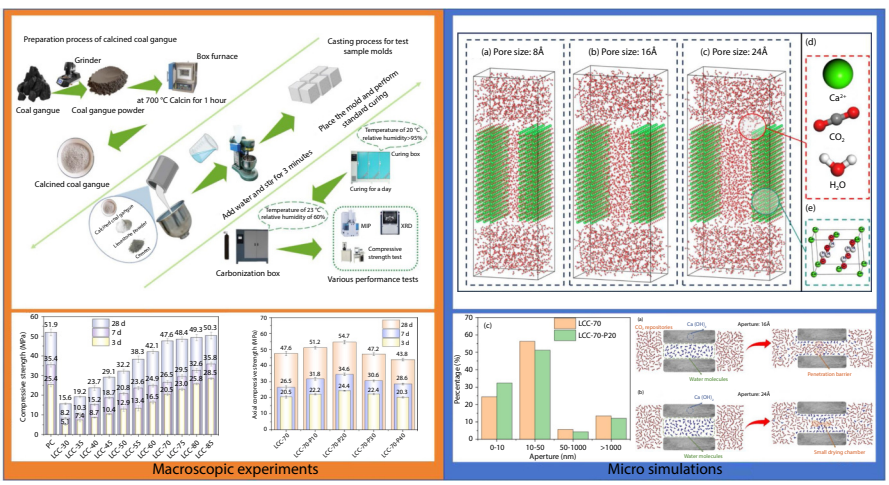

Keywords: Coal gangue, limestone calcined gangue cement, CO_2 mineralization conservation, pore structure optimization, green low-carbon cement

Citation: X. Zang, L. Zhang, D. Zhu, et al. Effects of CO_2 curing on hydration behavior, strength development, and microstructural evolution of coal gangue-based cementitious materials. *Materials Reports: Solidwaste and Ecomaterials*, 2026, 2: 9520024. https://doi.org/10.26599/MRSE.2026.9520024.

*Correspondence to L. Zhang, lzhan666@hebut.edu.cn; M. L. Nehdi, mnehdi@uoguelph.ca

Received 19 November 2025; Received in revised form 31 January 2026; Accepted 6 February 2026

1. Introduction

Coal has long been a pivotal energy source in China, occupying a central position in the national energy structure for decades. By 2020, China produced an estimated 3.8 billion tons of coal, accounting for nearly 47% of the world's total output[1]. However, the mining, washing, and processing of coal generate substantial amounts of solid waste, among which coal gangue is the primary by-product. According to statistics, the production of one ton of coal generates 100–150 kg of coal gangue[2-3]. Typically, these coal gangue wastes are stored directly without effective treatment, leading to severe environmental pollution. Therefore, recycling and utilization of coal gangue have become prominent research topics across various fields. Despite significant advancements in the comprehensive utilization of coal gangue in recent years, between 200 million and 400 million tons of coal gangue remain untreated annually, continually exacerbating environmental stress. Hence, there is an urgent need for efficient and feasible utilization technologies to mitigate ecological pressure[4].

In recent years, significant advances have been made in the valorization of coal gangue. For instance, Zhang et al.[5] found that coal gangue contains substantial amounts of clay minerals, specifically kaolinite, which, after high-temperature thermal activation, transforms into metakaolin exhibiting pozzolanic activity. This transformation allows its use as a supplementary cementitious material in cement production. Wu et al.[6] further noted that such conversion not only aids in consuming large quantities of discharged coal gangue but also effectively reduces carbon emissions and environmental pollution associated with cement production. With ongoing research, studies on the incorporation of calcined and activated coal gangue powder into cement have increased. Cheng et al.[7] demonstrated that the auxiliary cementitious material prepared from coal gangue activated at 700 °C by microwave for 50 min showed the highest compressive strength at 7 d, representing a 23.63% increase compared to that prepared from unactivated coal gangue. Additionally, Sui et al.[8] found that the reactivity of coal gangue increased initially and then decreased with rising calcination temperature, with an optimal range between 700 °C and 800 °C. Within this temperature range, kaolinite transforms into metakaolin, providing abundant reactive SiO_2, significantly promoting cement hydration reactions and strength enhancement. This implies that carefully controlling calcination temperature and duration can induce beneficial phase transformations in coal gangue minerals, thereby improving their reactivity and enhancing cement performance. Moreover, studies[9-13] indicated that incorporating calcined coal gangue powder into cement in appropriate proportions can enhance both early strength and long-term durability of the cement.

Currently, research into the CO_2 mineralization of coal gangue-based cement remains in preliminary stages, lacking systematic outcomes. Nevertheless, CO_2 mineralization curing technology has gained considerable attention as a sustainable and environmentally friendly curing method in recent years[14-16]. For example, Zuo et al.[17] argued that CO_2 mineralization curing of cement-based materials not only permanently stores CO_2 but also enhances mechanical strength and durability due to the filler and nucleation effects of mineralization products. Lin et al.[18] proposed an evaluation method for carbon fixation rates applicable to CO_2 mineralization-cured concrete, emphasizing the technology's capability to enhance mechanical properties and durability through mineralization reactions. Gu et al.[19] also found that CO_2 mineralization significantly improves the compressive strength and carbon fixation rates of aerated concrete while enhancing its durability. In summary, calcium hydroxide ($Ca(OH)_2$) within cement-based materials reacts with CO_2 to form calcium carbonate ($CaCO_3$), which improves density and strength. This curing method not only facilitates CO_2 sequestration but also significantly enhances the mechanical properties and durability of cement-based materials, providing a novel approach for their sustainable development.

Previous studies have demonstrated that CO_2 curing can enhance the compressive strength and durability of concrete to some extent. However, the effect of CO_2 curing on the properties of a novel ternary material—limestone-calcined coal gangue cement (LCC)—has not been specifically investigated. Therefore, a key challenge to address is how to integrate early-age CO_2 curing technology with the LCC to promote the application of coal gangue as a substitute for Portland cement, while simultaneously reducing fossil fuel consumption and the carbon footprint of cement production.

The calcined coal gangue-limestone composite cement, as a ternary cementitious system, achieves comparable mechanical strength to ordinary Portland cement while significantly enhancing concrete durability through the synergistic utilization of limestone and calcined clay in replacing conventional clinker. This study aims to investigate the mechanical properties and microstructure of cement-based materials prepared with calcined coal gangue and limestone as partial replacements for cement clinker, exploring the effects of CO_2 mineralization curing on cement-based materials. Additionally, $Ca(OH)_2$ is incorporated to enhance the performance of cementitious materials. Specifically, calcined coal gangue and limestone powder mixed at a ratio of 2:1 were used to partially replace cement. The study investigated the enhancement effect of $Ca(OH)_2$ on the mechanical properties of calcined coal gangue and identified optimal mixing ratios. X-ray diffraction (XRD) was used to characterize the hydration products of different admixtures, while mercury intrusion porosimetry (MIP) was employed to analyze the internal pore structure evolution under varying material compositions. Moreover, this study integrated experimental research with molecular dynamics simulations to thoroughly explore the preparation processes, performance optimization, and impacts of CO_2 mineralization curing on coal gangue-limestone cement. Through systematic experimental analyses and theoretical discussions, the study aims to provide scientific evidence and technical support for efficient coal gangue utilization and sustainable, low-carbon development of cement-based materials.

2. Materials and methods

2.1. Experimental materials

The coal gangue powder used in this study was sourced from the Huafeng Coal Mine located in Shandong Province, China. The cement utilized was P·I 52.5 cement due to its enhanced corrosion resistance and optimized particle size distribution. The limestone powder, produced by manufacturers in Beichen District, Tianjin, China, consisted of ultra-white heavy calcium carbonate. Their chemical compositions are detailed in Table 1.

2.2. Activation treatment of coal gangue

Thermogravimetric analysis was performed on the coal gangue powder. Fig. 1 shows the derivative thermogravimetric (DTG) curve, indicating a significant mass loss within the temperature range of 400–750 °C. This weight reduction is primarily attributed to the dehydroxylation of kaolinite (400–700 °C) and illite (700–800 °C). Thus, activation involved heating coal gangue powder (with particle sizes less than 45 μm) in a furnace at 700 °C for 1 h. From the XRD patterns of coal gangue powder in Fig. 2, the primary mineral phases identified are quartz, kaolinite, and illite. Post-calcination, the XRD peaks of kaolinite disappeared, and the crystallinity significantly decreased.

Based on the mass loss in the temperature range of 400–700 °C, the content of kaolinite in the coal gangue was quantitatively determined to be 10.31% using the tangent method[20]. This method can be briefly summarized as follows: coal gangue samples of known mass were heated in the TGA instrument from ambient temperature to 700 °C, with continuous recording of mass loss. A tangent baseline was drawn on the TGA curve (Fig. 1) to analyze the significant mass loss between 400 °C and 700 °C, primarily due to the dehydroxylation of kaolinite, which corresponds to the theoretical mass change of undecomposed kaolinite. The actual mass loss attributed to kaolinite was determined by subtracting the baseline thermal mass loss from the total observed loss within the relevant temperature range. Based on the stoichiometry of kaolinite dehydroxylation, the corrected mass loss was subsequently converted to the corresponding kaolinite content.

2.3. Preparation and curing of specimens

Based on existing research on limestone-calcined coal gangue cement[21], a calcined coal gangue to limestone powder ratio of 2:1 was adopted for this study. The limestone-calcined coal gangue cement is denoted as LCC-*X*, where *X* represents the cement clinker content in the cementitious material; the specific proportions are listed in Table 2.

To prepare the specimens, the raw materials were mixed thoroughly in a mixer, followed by the gradual addition of water and continued mixing for an additional 3 min. The resulting mixture was then cast into molds measuring 40 mm × 40 mm × 40 mm and cured in a standard curing chamber (20 ± 2 °C, relative humidity > 95%) for 24 h prior to demolding. After demolding, the specimens were cured in a carbonation chamber for 3, 7, and 28 d (temperature of 23 °C, relative humidity of 60%, and CO_2 concentration of 10%) for subsequent compressive strength and microstructural testing. The preparation process is illustrated in Fig. 3. In the experimental design, the thermal treatment of coal gangue was conducted at nearly 700 °C using an SX2 intelligent muffle furnace, with a heating rate of 11.25 °C min^{-1}, followed by a one-hour isothermal hold. Subsequently, the ambient temperature cooling method was employed to achieve temperature reduction. Throughout the process, strict adherence to predefined mixing ratios was maintained to ensure consistency and accuracy. Initially, all powder materials were thoroughly dry-mixed to achieve homogeneity, followed by the controlled addition of water in accordance with standardized protocols.

3. Molecular dynamics simulation study

3.1. Simulation methods

Large-scale Atomic/Molecular Massively Parallel Simulator (LAMMPS) was used to investigate CO_2 diffusion in three different calcium hydroxide ($Ca(OH)_2$) structures. The crystal structures were obtained from the Inorganic Crystal Structure Database. Based on this structure, the unit cell was expanded into a supercell measuring 65 Å × 35 Å × 15 Å, as illustrated in Fig. 4. The pore sizes were set at 8 Å, 16 Å, and 24 Å, with a water density at 0.60 g cm^{-3}, resembling humid conditions with intermediate characteristics between liquid and gas. Additionally, two CO_2 reservoirs, each measuring 35 Å × 35 Å × 40 Å, were used. CO_2 molecule density was set at 567 kg cm^{-3}, corresponding to the conditions of 25 °C (298.15 K) and 1 MPa (10 bar). Fig. 5 shows the simulation model.

Given the broad applicability of $Ca(OH)_2$ in clay and cement-based materials, an interface force field (IFF) was employed to simulate $Ca(OH)_2$ surface behavior and surface charges[22]. The SMART (Simultaneous Minimization and Reaction Tuning) method, combining steepest descent, conjugate gradient, and Newton-Raphson methods, was used for system optimization. Dynamic simulations were conducted in the NVT ensemble (constant number of particles, volume, and temperature) at 298 K for 1 ns. The system stabilized after 300 ps, and the reported results were based on data after this period. A time step of 0.1 fs and periodic boundary conditions were employed to minimize boundary effects. CO_2 adsorption and diffusion behavior were evaluated based on pore sizes and the presence of internal water.

Table 1. Chemical composition of cement, coal gangue powder, and limestone (%).

Material	CaO	SiO_2	Al_2O_3	Fe_2O_3	MgO	Na_2O	K_2O	SO_3	TiO_2	$CaCO_3$
Cement	69.58	16.42	4.77	3.10	1.72	0.20	0.60	2.64	0.47	-
Coal gangue powder	3.9	50.5	29.1	6.6	1.3	1.3	0.8	-	-	-
Limestone	-	0.3	0.012	0.02	1.6	-	-	-	-	95.3

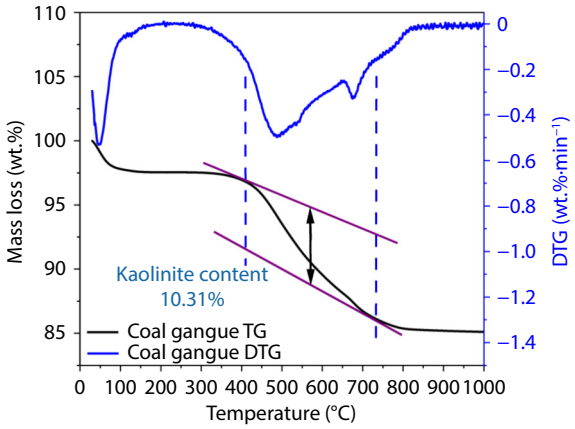

Fig. 1. TGA curves of coal gangue mass loss.

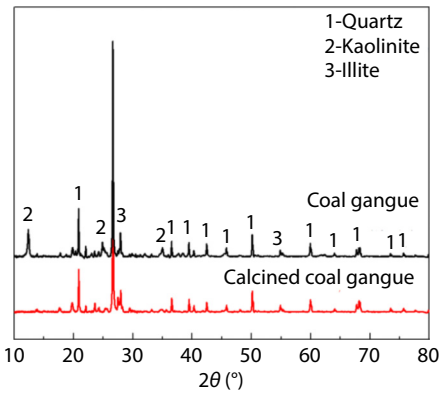

Fig. 2. XRD spectra of raw coal gangue and calcined ones at 700 °C.

3.2. Interface force field

In molecular dynamics, the interface force field (IFF) describes interactions at various material interfaces (such as liquid-solid, liquid-gas, or solid-gas). IFF specifies potential energy for atom or molecule interactions, specifically addressing interfacial heterogeneities. The interface region typically involves interactions between multiple materials or phases, requiring IFF to account for van der Waals forces, electrostatic interactions, hydrogen bonds, and other interactions. IFF must consider atomic force field parameters of each phase and interphase effects, including molecular adsorption, interfacial tension, and dissolution phenomena[23].

Table 2. Proportion of mixed cementitious materials (%).

Number	Cement	Calcined coal gangue	Limestone powder	Water
LCC-30	30	47	23	45
LCC-35	35	43	22	45
LCC-40	40	40	20	45
LCC-45	45	37	18	45
LCC-50	50	33	17	45
LCC-55	55	30	15	45
LCC-60	60	27	13	45
LCC-70	70	20	10	45
LCC-75	75	17	8	45
LCC-80	80	13	7	45
LCC-85	85	10	5	45
PC	100	0	0	45

3.3. Adsorption-induced polymerization degree

Statistics on under- and over-coordination of atoms are foundational for polymerization reaction studies. The coordination number refers to the relative position relationships between atoms and neighboring atoms, typically describing atomic coordination environments. Specifically, it represents the number of bonds formed by an atom within a given radius.

Radial distribution function (RDF) was employed to determine the cutoff radius for statistical under- and over-coordina-

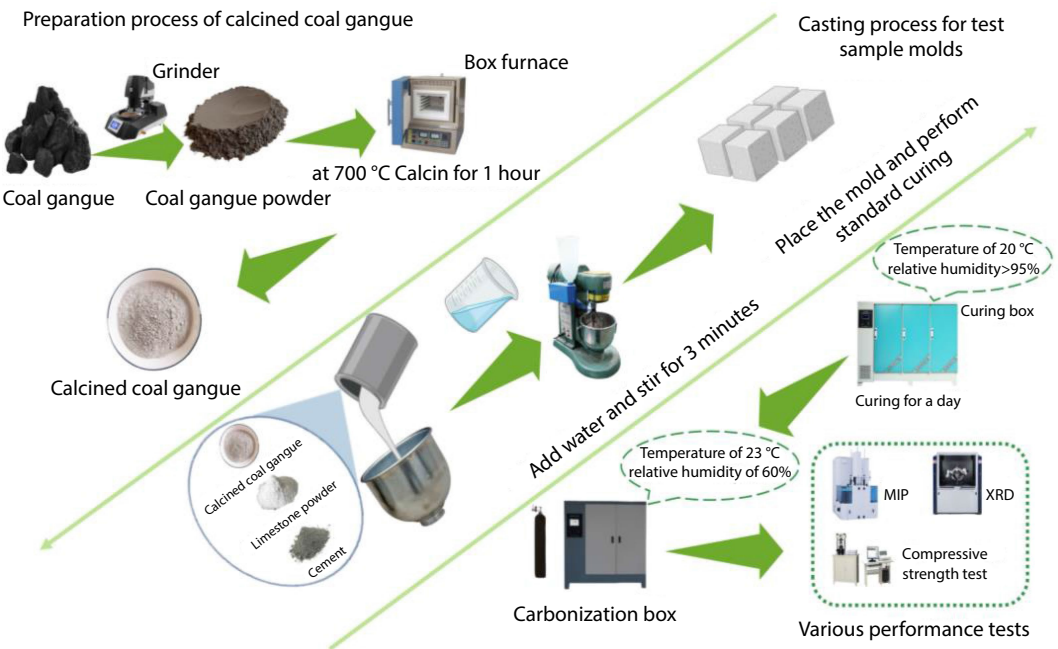

Fig. 3. Experimental procedure for preparing limestone–calcined coal gangue cement.

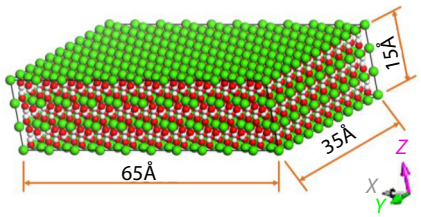

Fig. 4. Cellular structure of portlandite.

tion of atom pairs. RDF is critical in molecular dynamics studies, reflecting the probability of finding other atoms around a target atom within a specific region as a function of radial distance, $g(r)$. The RDF is related to functions obtained from X-ray small-angle diffraction experiments via Fourier transforms, as shown in Equation (1)[24]:

$$g(r) = \frac{n(r)}{\rho v} \approx \frac{n(r)p}{4\pi r^2 \delta(r)\rho} \quad (1)$$

where r is the radial distance, $n(r)$ is the number of atoms within the spherical shell, ρ is the crystal density, and $\delta(r)$ is the shell thickness. RDF curve analysis identified the first local minimum after the initial peak as the cutoff radius for atom pair bonding distances, with detailed RDF results provided in Section 4.4.

4. Results and discussion

4.1. Effect of calcined coal gangue content on the compressive strength of coal gangue-based cement

Fig. 6 illustrates the compressive strength of the limestone-calcined coal gangue cement cured under CO_2 mineralization and ordinary Portland cement (PC) at different curing ages (3, 7, and 28 d). As the cement content decreases from LCC-85 to LCC-30, the compressive strength progressively declines. This decline is primarily attributed to the increased relative proportions of calcined coal gangue and limestone powder, which possess lower reactivity and thus negatively impact strength development at all ages.

Studies indicate that incorporating 30% calcined coal gangue as a supplementary cementitious material results in an approximately 16% reduction in the 28-day compressive strength of concrete under identical mix proportions[21]. Nevertheless, at 28 days, both LCC-85 and LCC-70 in this trial exhibited excellent compressive strengths of 50.3 MPa and 47.6 MPa, respectively, which were close to the 28-day strength of PC (51.9 MPa). This outcome can be explained by the reaction between $Ca(OH)_2$ and CO_2. During cement hydration, approximately 0.25 kg of $Ca(OH)_2$ is produced per kg of cement[25]. In the CO_2 mineralization curing process, $Ca(OH)_2$ reacts with CO_2 to form $CaCO_3$ and H_2O, as described by the following chemical equation:

$$Ca(OH)_2 + CO_2 \rightarrow CaCO_3 \downarrow + H_2O \quad (2)$$

The formation of $CaCO_3$ enhances material densification by filling internal pores, significantly increasing compressive strength. Therefore, the carbonation of $Ca(OH)_2$ plays a crucial role in improving the strength of limestone-calcined coal gangue cement composites. This finding suggests that optimizing the $Ca(OH)_2$ content may further enhance the mechanical performance. The subsequent section explores the influence of $Ca(OH)_2$ admixture on the microstructure and mechanical properties of these composites to provide theoretical and technical support for practical optimization.

4.2. Influence of calcium hydroxide admixture on mechanical properties of coal gangue-based cement

Based on the aforementioned research, among all LCC mix proportions, when the cement clinker content decreased from 100% to 70%, the 28-day compressive strength decreased from 51.9 MPa to 47.6 MPa—a reduction of 8.3%, which is below the 10% threshold. This meets the requirement specified in GB/T 12957-2005, Test method for activity of indus-

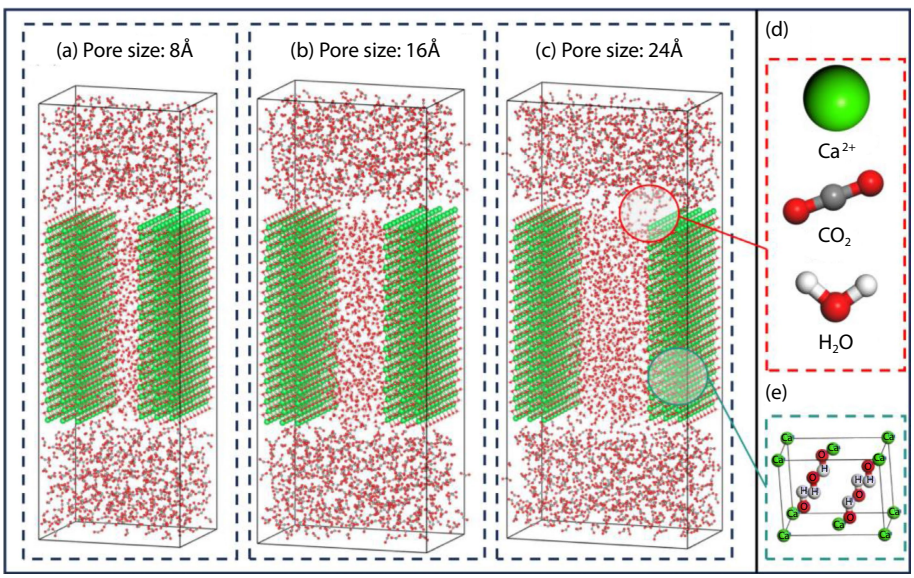

Fig. 5. Three-dimensional view of the three models: (a–c) Portlandite with varied pore sizes, (d) Molecular and ionic building blocks of porous portlandite, (e) Crystal structure of portlandite.

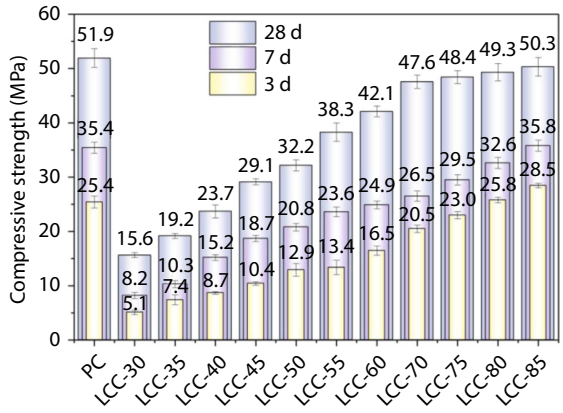

Fig. 6. Compressive strength of limestone–calcined coal gangue cement at 3, 7, and 28 d.

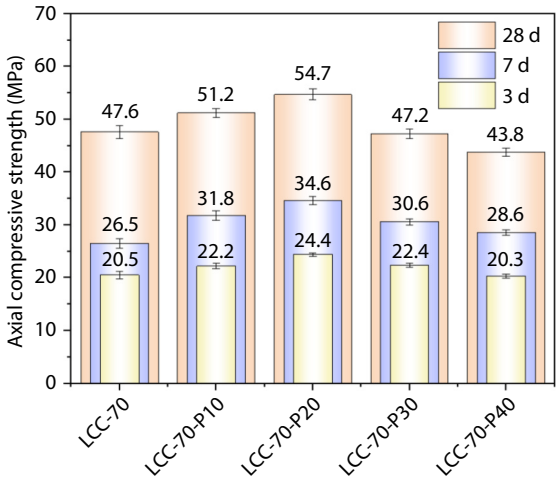

Fig. 7. Compressive strength development of limestone–calcined coal gangue cement mixtures with and without $Ca(OH)_2$ at 3, 7, and 28 d.

trial waste slag used as addition to cement, that the activity index should be ⩾ 90%. Therefore, LCC-70 is confirmed as the critical mix proportion that maintains the strength grade even under high substitution rates.

To investigate the impact of additional $Ca(OH)_2$ on compressive strength, various amounts of $Ca(OH)_2$ were introduced into the LCC system (denoted as LCC-P*X*, where *X* is the percentage of $Ca(OH)_2$ relative to calcined coal gangue). Table 3 details the mix design. It should be noted that the proportion of $Ca(OH)_2$ content was determined based on the mix design reported by Kong et al.[26], with the aim of using the 28-day uncarbonated curing strength data from their study as a blank control.

Fig. 7 presents the effect of different $Ca(OH)_2$ additions on the compressive strength of LCC-70 mixtures at curing ages of 3, 7, and 28 d. It can be observed that an appropriate dosage of $Ca(OH)_2$ (e.g., LCC-70-P10 and LCC-70-P20) significantly enhances the compressive strength of the mixtures.

Table 3. Mixture proportion of limestone–calcined coal gangue cement with $Ca(OH)_2$ (%).

Number	Cement	Calcined coal gangue	Limestone	$Ca(OH)_2$	Water
LCC-70	70	20	10	0	45
LCC-70-P10	68.63	19.61	9.80	1.96	45
LCC-70-P20	67.30	19.23	9.62	3.85	45
LCC-70-P30	66.04	18.87	9.43	5.66	45
LCC-70-P40	64.81	18.52	9.26	7.41	45

Specifically, the 28-day compressive strength of LCC-70-P10 was 51.2 MPa, representing an increase of approximately 7.6% compared to LCC-70. Meanwhile, LCC-70-P20 achieved a strength of 54.7 MPa, corresponding to an enhancement of about 14.9% relative to LCC-70. This improvement can be attributed to the reaction between $Ca(OH)_2$ and CO_2 during the carbonation process, which generates $CaCO_3$. The formed $CaCO_3$ fills the micropores within the concrete, reduces internal defects, and leads to a denser microstructure. This densified structure effectively contributes to the increased compressive strength of the concrete.

However, when the dosage of $Ca(OH)_2$ exceeds a certain threshold (e.g., LCC-70-P30 and LCC-70-P40), the compressive strength shows a decrease. For instance, the 28-day compressive strength of LCC-70-P30 was 47.2 MPa, approximately 0.8% lower than that of LCC-70. In contrast, LCC-70-P40 exhibited a strength of 43.8 MPa, representing a more significant reduction of about 8.0% compared to LCC-70. This decline is likely attributable to the excessive $Ca(OH)_2$, which may promote an excessive formation of $CaCO_3$ within the concrete. The generation of excessive $CaCO_3$ could induce local expansion, leading to the formation of micropores. These micropores compromise the compactness of the concrete, thereby reducing its compressive strength. As observed in the scanning electron microscopy (SEM) images in Fig. 8, the LCC-70-P40 group displays a relatively cracked microstruc-

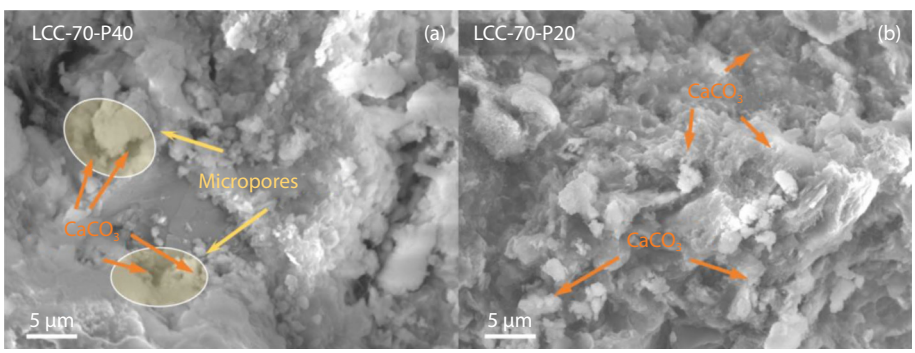

Fig. 8. Scanning electron microscopy images of different mixtures.

ture with pore sizes around 3–4 μm. In contrast, the LCC-70-P20 group shows substantial precipitation of $CaCO_3$ on the surfaces of C-S-H gels, with pores nearly completely filled, resulting in a significantly denser microstructure. This observation aligns with the compressive strength analysis, indicating that LCC-70-P20 facilitated the formation of well-crystallized and appropriately distributed $CaCO_3$ during CO_2 curing. This demonstrates that an appropriate additional amount of $Ca(OH)_2$ plays a crucial role in enhancing both early-age and later-age strength. The presence of $Ca(OH)_2$ not only promotes the formation of more hydration products but also reduces porosity through the mineralization reaction that generates $CaCO_3$, thereby improving the mechanical properties of the cementitious material, as evidenced by the XRD patterns in Fig. 9.

XRD analysis confirmed the presence of $Ca(OH)_2$ in all mixtures at both 3 and 7 d. At 3 d, distinct peaks corresponding to monocarboaluminate (MC) and residual $Ca(OH)_2$ were observed. In these systems, tricalcium aluminate (C_3A) reacts with $CaCO_3$ derived from limestone to form monocarbonate phases. Additionally, in the limestone-calcined coal gangue cement system, reactive alumina released from calcined gangue further participates in the reactions with limestone and $Ca(OH)_2$, contributing to the formation of additional monocarbonate[27]. Notably, the absence of significant ettringite peaks in Fig. 9 can be attributed to the dissolution of calcined coal gangue, which releases reactive ions such as SiO_4^{4-} and AlO_2^-[28]. These ions interact with Ca^{2+} and OH^- in the solution to form hydration products such as calcium silicate hydrate (C-S-H) and calcium aluminosilicate hydrate (C-A-S-H). Consequently, the substantial consumption of Ca^{2+} and OH^- in the pozzolanic reaction of calcined coal gangue limits the availability of these ions for ettringite formation, resulting in its diminished presence[29].

Based on the XRD analysis, the characteristic $Ca(OH)_2$ peaks in LCC-70 and LCC-70-P10 completely disappear after 28 d of coupled hydration and carbonation reactions, which can be explained by two concurrent mechanisms: the complete consumption of portlandite through pozzolanic reactions involving calcined coal gangue, and its additional depletion via carbonation processes. In contrast, the LCC-70-P30 and LCC-70-P40 systems retain detectable $Ca(OH)_2$ residues at 28 days due to their excessive initial addition, in which the unreacted surplus not only fails to contribute to strength development but may also negatively impact the microstructure, ultimately leading to the observed reduction in compressive strength. This phenomenon further confirms that an optimal $Ca(OH)_2$ dosage is crucial for balancing reaction kinetics and mechanical performance in this cementitious system.

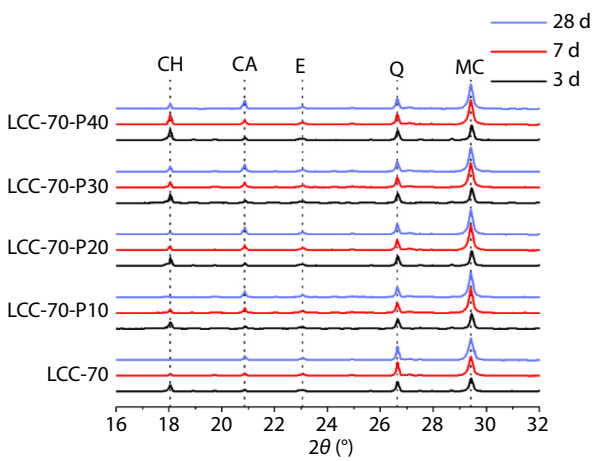

Fig. 9. XRD patterns of LCC-70 mixtures with different $Ca(OH)_2$ contents at 3, 7, and 28 d, showing the presence of major hydration products such as calcium hydroxide (CH), calcite (CA), calcite (E), quartz (Q), and monocarboaluminate (MC).

4.3. Effect of calcium hydroxide on the pore structure of coal gangue-based cement

The pore structures of LCC-70 and LCC-70-P20 samples after 28 d of hydration were characterized using MIP (Fig. 10). As shown in Fig. 10a, the LCC-70 sample exhibits prominent peaks around 20 nm and 50 nm, indicating a higher specific volume of larger pores. In contrast, the LCC-70-P20 sample displays distinct peaks near 10 nm and 20 nm, suggesting an increased specific volume within this size range compared to LCC-70. The presence of smaller pores likely contributes to a lower total porosity, which is further confirmed by the cumulative porosity data in Fig. 10b. Quantitative analysis reveals that LCC-70 has a total porosity of 24.8%, while LCC-70-P20 demonstrates a reduced porosity of 21.9%. This reduction suggests that the addition of $Ca(OH)_2$ enhances carbonation reactions, leading to the formation of additional $CaCO_3$ and consequent refinement of the pore structure. This interpretation is further supported by Fig. 10c, which reveals that LCC-70-P20 contains a higher proportion of pores in the 0–10 nm range compared to LCC-70.

Investigating the influence of different pore types on carbonation reactions is crucial for gaining fundamental insights into the compressive strength and long-term performance of cementitious materials. Distinct pore categories exhibit markedly different effects on carbonation mechanisms. Specifically, gel pores (< 10 nm) significantly enhance the reaction kinetics by providing increased specific surface area for CO_2 adsorption and subsequent reaction interfaces, thereby accelerating carbonation progress[30]. Transition pores (10–50 nm), located primarily in the interfacial transition zones, facilitate CO_2 penetration through interconnected channels, enabling progressive carbonation advancement despite their relatively slower reaction rates[31]. Capillary pores (50–1000 nm) serve as primary pathways for both moisture and CO_2 transport, effectively promoting carbonation propagation throughout the matrix[32]. While macropores (> 1000 nm) do not directly participate in carbonation reactions, they critically influence the mechanical integrity and structural stability of the cementitious system. Under environmental stressors such as freeze-thaw cycles or wet-dry alternations, these larger voids may exacerbate material degradation, indirectly facilitating carbonation penetration[33]. This comprehensive pore structure analysis provides a mechanistic explanation for the superior compressive strength of LCC-70-P20 compared to LCC-70 at 3, 7, and 28 d, as demonstrated in Fig. 7.

In mercury intrusion porosimetry (MIP), technological limi-

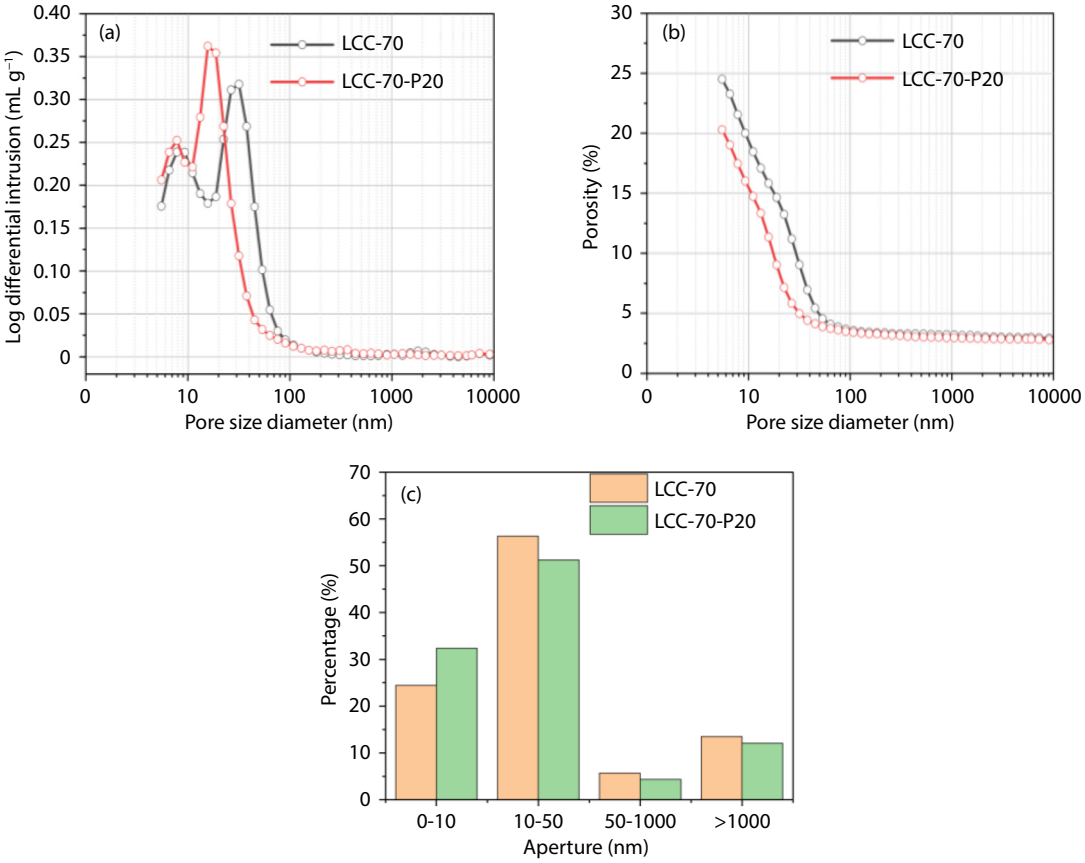

Fig. 10. Pore structure analysis of limestone–calcined coal gangue cement mixtures with different $Ca(OH)_2$ contents: (a) different pore size distributions; (b) porosity distributions; and (c) pore size classification of LCC-70 and LCC-70-P20 at 28 d.

tations prevent accurate measurement of pore structures below 5 nm in concrete, particularly when evaluating CO_2 sequestration effects. To address this fundamental gap, molecular dynamics (MD) simulations were employed in the following section to complement experimental data. This computational approach provides atomic-scale resolution for investigating pore structure effects on carbonation processes, especially within the critical sub-nanometer range. Specifically, the simulation examined pore diameters of 8 Å, 16 Å, and 24 Å (corresponding to 0.8 nm, 1.6 nm, and 2.4 nm, respectively) to systematically evaluate their influence on the reaction between $Ca(OH)_2$ and CO_2. These simulations establish a theoretical framework for understanding how concrete pore architecture governs carbonation efficiency. The subsequent discussion will first address the experimental observations of the impact of $Ca(OH)_2$ on concrete pore structure, followed by mechanistic interpretations from the MD simulations regarding pore-size-dependent carbonation pathways.

4.4. Molecular dynamics insight into the effect of pore size on carbonation curing

The evolution of computational algorithms and hardware capabilities has positioned numerical simulation as a feasible approach to complement or substitute experimental studies. In this context, molecular dynamics simulation has garnered considerable interest due to its ability to serve as a high-fidelity computational tool for probing CO_2 carbonation mechanisms at the atomic level. For example, Qin et al.[34] utilized molecular dynamics simulations to examine how the silicon-to-aluminum ratio influences the carbonation kinetics in cementitious systems. The work of Mutisya and Kalinichev[35], employing molecular dynamics simulations, indicated that cement-water interactions facilitate the formation of an interfacial water film on solid surfaces, which subsequently restricts CO_2 diffusion. Similarly, through reactive and classical molecular dynamics simulations, Qin et al.[36] investigated the nucleation mechanism of $CaCO_3$ during the carbonation process. While these simulation studies offer reliable insights for capturing and reconstructing critical stages of CO_2 carbonation, a comprehensive understanding of the atomic-scale mechanisms governing CO_2 diffusion, adsorption, and reaction within concrete pores remains a significant knowledge gap. To address this gap, the present study was initiated with the objective of elucidating the mechanisms of CO_2 diffusion within nanoporous environments. It should be emphasized that the 1 ns timeframe of the molecular dynamics simulation cannot be directly correlated with the 28-day carbonation process in the experiments; therefore, this simulation serves solely for comparative trend analysis.

Molecular dynamics simulations revealed that the transport of CO_2 molecules through the porous cementitious matrix constitutes the fundamental process underlying carbonation curing[37]. For the carbonation reaction to initiate, the migrating CO_2 must first establish contact with and adsorb onto the silicate surfaces within the cement matrix pores. Fig. 11a presents a representative simulation model combining

one reservoir with a portlandite ($Ca(OH)_2$) cavity, illustrating this interfacial interaction.

During CO_2 injection, the concentration distribution of CO_2 molecules within water-saturated pores is illustrated in Fig. 11c, e, and g. The simulations reveal distinct CO_2 reservoirs forming in the 0–35 Å and 100–135 Å regions, while the intermediate pore zone (35–100 Å) remains predominantly occupied by the portlandite ($Ca(OH)_2$) model and water molecules. Initial conditions show zero CO_2 concentration, confirming the absence of pre-existing carbon dioxide in the pore system prior to injection. As the injection progresses, a gradual increase in CO_2 concentration is observed throughout the pore network.

The study reveals a pore-size-dependent evolution of CO_2 concentration distribution. In confined pores of 8 Å and 16 Å diameters, CO_2 exhibits relatively lower concentration with characteristic high-low-high axial distribution profiles, indicating significant molecular water blocking effects—a phenomenon consistent with Wang et al.'s findings[38]. Conversely, the 24 Å cavity demonstrates substantially enhanced CO_2 concentration. Particularly in narrower pores, structured water layers markedly reduce CO_2 diffusion and exchange efficiency through modification of interfacial hydration structures.

The molecular dynamics simulations reveal distinct confinement effects on water structure and CO_2 diffusion behavior in portlandite ($Ca(OH)_2$) cavities. In the 8 Å and 16 Å cavities, water molecules form a densely packed network that

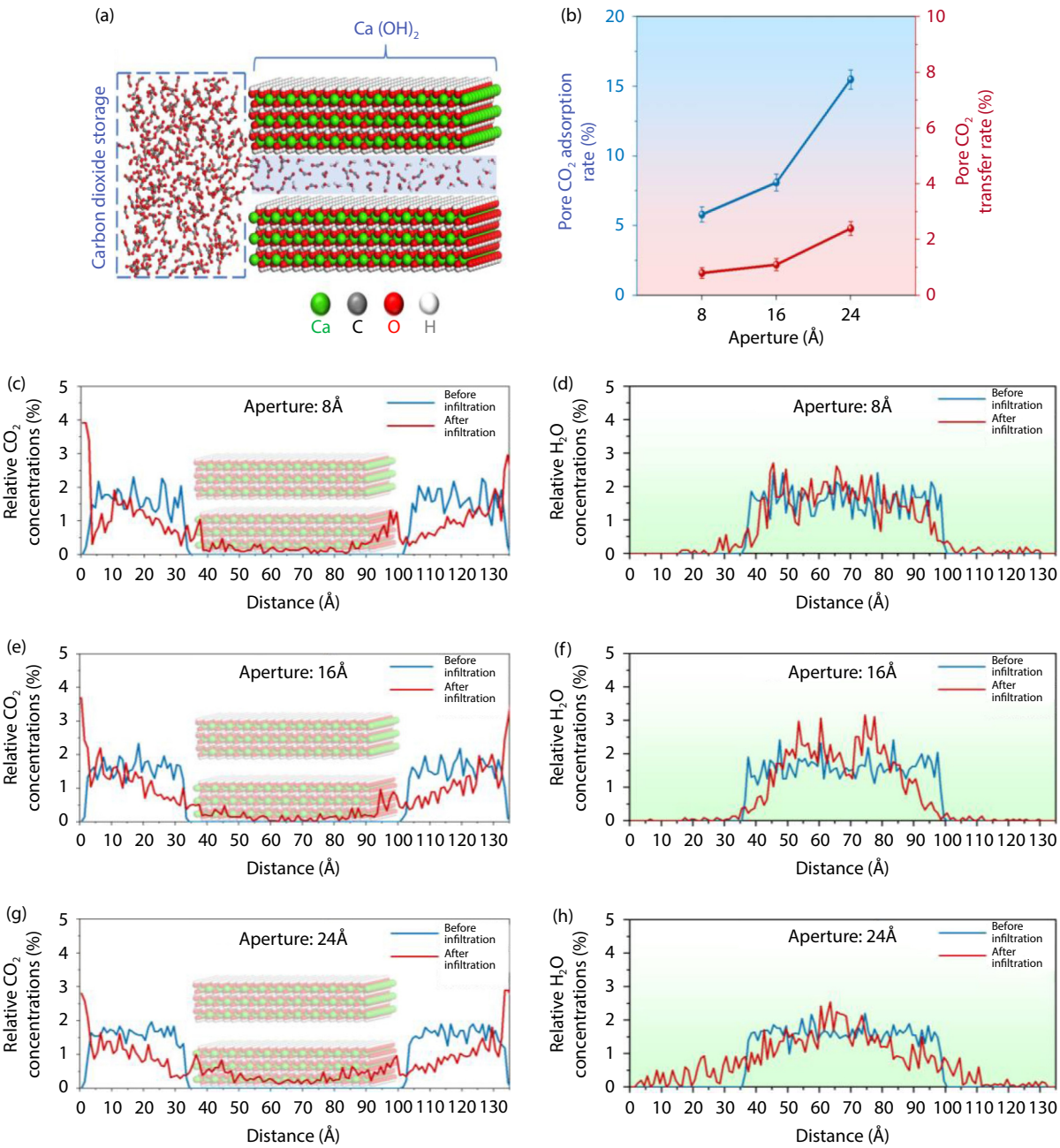

Fig. 11. (a) CO_2 molecule and portlandite wet cavity models; (b) CO_2 adsorption and transfer rates between hydrotalcite layers; (c–h) relative CO_2 and H_2O concentrations in three models with pore sizes of 8, 16, and 24 Å, respectively.

effectively occupies the available pore space. This ordered structure, stabilized by extensive hydrogen bonding between water molecules and surface hydroxyl groups of portlandite, creates a significant diffusion barrier for CO_2 molecules[39]. As illustrated in Fig. 11d, f, and h, the compact water arrangement leaves minimal free volume for CO_2 migration, substantially impairing its transport efficiency through the silicate matrix. In contrast, while the 24 Å cavity contains more water molecules, the increased pore volume results in weaker intermolecular interactions that prevent the formation of a continuous blocking network[40]. Fig. 12 quantitatively demonstrates how the larger pore diameter provides alternative diffusion pathways, enabling CO_2 molecules to circumvent aqueous obstacles and diffuse more efficiently through the portlandite structure. This size-dependent behavior explains the observed enhancement in carbonation efficiency with increasing pore dimensions.

Fig. 11b demonstrates the pore-size-dependent CO_2 adsorption and transport behavior. The CO_2 adsorption capacity shows a progressive enhancement as the cavity height increases from 8 Å to 24 Å, indicating that larger cavities provide more available space and additional adsorption sites for CO_2 molecules[41]. Particularly in the 24 Å cavity, the reduced confinement effect significantly diminishes the obstructive influence of water molecules on CO_2, resulting in optimal adsorption and transport efficiency. Complementing these findings, Fig. 13 reveals a remarkable intensification of Ca^{2+}-C interaction peaks at 2.7 Å and 3.2 Å with increasing pore size from 8 Å to 24 Å. The strongest peaks occur in the 24 Å cavity, demonstrating that expanded pore dimensions facilitate more frequent and effective interactions between calcium and carbon atoms. This atomic-scale evidence directly correlates with the macroscopic observations of enhanced CO_2 adsorption and transport efficiency in larger pores, providing a coherent multiscale understanding of the pore-size-dependent carbonation mechanism.

In summary, pore height emerges as a critical factor governing CO_2 adsorption and transport behavior in hydrated silicate cavities. Larger cavities not only enhance CO_2 adsorption capacity but also significantly improve its diffusion and transport characteristics within the pore network. As the cavity height increases, the obstructive effect of water molecules progressively diminishes, thereby amplifying the carbonation and solidification efficiency of CO_2 within the silicate matrix. These fundamental insights suggest that strategic optimization of pore architecture, particularly through controlled pore height engineering, could substantially improve CO_2 sequestration efficiency in practical applications.

The findings of this study suggest that CO_2 curing can be an effective strategy to accelerate early-age densification and strength development of limestone-calcined coal gangue-Portland cement binders when an appropriate $Ca(OH)_2$ dosage is provided, indicating potential applicability for precast elements where curing conditions can be tightly controlled. Nevertheless, several limitations should be acknowledged. First, the CO_2-curing performance is sensitive to the boundary conditions (CO_2 concentration/pressure, relative humidity, and curing duration), and scale-up may introduce non-uniform CO_2 penetration and carbonation gradients in larger components. Second, implementation requires sealed curing chambers and operational safety measures, which may affect cost and feasibility depending on the production line. Third, the net carbon benefit depends on the CO_2 source and the energy demand of gas supply and chamber operation; a full life-cycle assessment was beyond the scope of this work and will be addressed in future studies. Finally, variability in calcined coal gangue may influence hydration/carbonation kinetics, and the long-term durability under service environments needs further systematic evaluation.

5. Conclusions

This study highlights the essential role of CO_2 curing in accelerating strength development and improving microstructural refinement in coal gangue-based low-carbon cementitious materials. Through a combined experimental and simulation framework, the feasibility of utilizing calcined coal gangue as

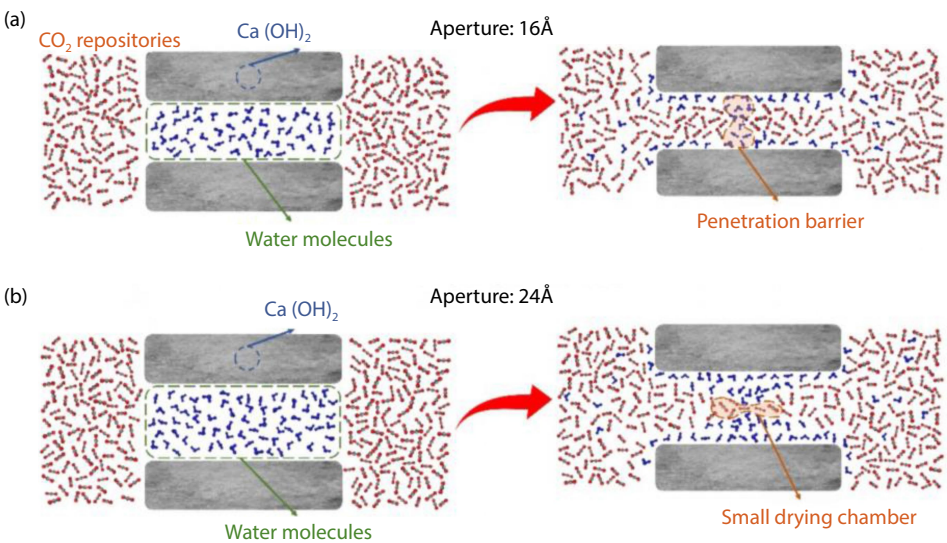

Fig. 12. Snapshot of the high permeability process in (a) 16 Å pore and (b) 24 Å pore.

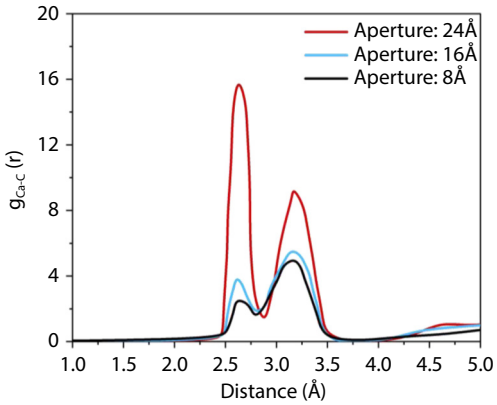

Fig. 13. Radial distribution function diagram of Ca–C bonds.

a sustainable clinker alternative is systematically verified. The key findings and conclusions of this study can be summarized as follows:

(1) Calcined coal gangue can be effectively incorporated into cementitious systems as a sustainable partial replacement for clinker, achieving improved mechanical performance and refined microstructure when optimized with limestone powder and mix design.

(2) CO_2 curing markedly enhances the early compressive strength of limestone-calcined coal gangue cement, demonstrating strong potential for low-carbon and performance-enhanced cement manufacturing.

(3) The addition of $Ca(OH)_2$ plays a crucial role in strengthening the composite system; an appropriate dosage promotes $CaCO_3$ precipitation during carbonation, filling micropores, reducing porosity, and increasing matrix compactness. However, excessive $Ca(OH)_2$ may trigger localized expansion and the formation of micropores.

(4) MIP analyses and molecular dynamics simulations reveal that pore size distribution strongly governs CO_2 transport and mineralization efficiency. Ultra-fine pores (8–16 Å) restrict CO_2 mobility due to confined water structure, whereas larger pores (~24 Å) facilitate gas diffusion and adsorption, accelerating carbonation reactions.

(5) CO_2 curing provides dual environmental and mechanical benefits by simultaneously improving material strength and permanently storing CO_2 within reaction products, significantly reducing the carbon footprint of the cement system.

Overall, integrating CO_2 curing into the limestone-calcined coal gangue-Portland cement system offers a practically relevant pathway to simultaneously promote early-age densification and carbonation-assisted hydration, thereby enabling higher clinker substitution with an improved strength-durability balance under controlled curing conditions. The results indicate that a moderate $Ca(OH)_2$ dosage window is preferable to maximize the benefit of CO_2 curing while avoiding diminishing returns associated with excessive portlandite and transport hindrance, and the observed improvements can be rationalized by the coupled experimental evidence together with the pore-size-dependent CO_2 diffusion trends revealed by molecular simulations. However, for engineering deployment, potential scale-up constraints should be recognized, including CO_2 penetration gradients and carbonation non-uniformity in larger components, the requirement for sealed curing chambers and safety control, and the dependence of net carbon benefit on CO_2 source purity and the energy demand of the curing process. Therefore, future work should focus on validating performance at larger scales and under realistic curing atmospheres, establishing robust process windows, and conducting systematic long-term durability assessments together with comprehensive life-cycle sustainability evaluation to confirm the field applicability of this low-carbon binder technology.

Author contribution statement

Xuyang Zang: Writing – original draft, Methodology, Data curation. **Lei Zhang:** Writing – original draft, Supervision, Funding acquisition, Conceptualization. **Dehui Zhu:** Writing – review & editing, Investigation, Formal analysis. **Zhijun Li:** Writing – review & editing. **Tao Li:** Resources, Data curation. **Yitong Ren:** Visualization, Data curation. **Moncef L. Nehdi:** Methodology, Project administration.

Declaration of competing interest

The authors declare the following financial interests/personal relationships which may be considered as potential competing interests: Tao Li is employed by Inner Mongolia Long'an Safety Assessment Co., Ltd.

Acknowledgements

The authors would like to acknowledge the support provided by the S&T Program of Hebei (Grant No.: E2024202247).

References

[1] Sun, H., Wang, S., Zhao, Y., et al. Exploring the carbon neutrality pathway in the aluminum industry from the perspective of energy-environment-economy: A case study of Henan Province, China. *International Journal of Greenhouse Gas Control*, **2025**, 144: 104375. https://doi.org/10.1016/j.ijggc.2025.104375.

[2] Zhang, L., Zhu, D., Marani, A., et al. Toward sustainable construction: Comprehensive utilization of coal gangue in building materials. *Case Studies in Construction Materials*, **2025**, 23: e04930. https://doi.org/10.1016/j.cscm.2025.e04930.

[3] Gao, L., Liu, Y., Xu, K., et al. A short review of the sustainable utilization of coal gangue in environmental applications. *RSC Advances*, **2024**, 14(53): 39285–39296. https://doi.org/10.1039/d4ra06071g.

[4] Zheng, Q., Zhou, Y., Liu, X., et al. Environmental hazards and comprehensive utilization of solid waste coal gangue. *Progress in Natural Science: Materials International*, **2024**, 34(2): 223–239. https://doi.org/10.1016/j.pnsc.2024.02.012.

[5] Zhang, K., Yang, Y., Li, H. Cementitious properties of coal-based metakaolin prepared from coal gangue *via* Fe_3O_4-Assisted microwave activation. *Journal of Cleaner Production*, **2024**, 448: 141277. https://doi.org/10.1016/j.jclepro.2024.141277.

[6] Wu, H., Chen, C., Song, W., et al. High-capacity utilization of coal gangue as supplementary cementitious material, geopolymer, and aggregate: A review. *Construction and Building Materials*, **2024**, 435: 136857. https://doi.org/10.1016/j.conbuildmat.2024.136857.

[7] Cheng, S., Wang, H., Feng, C., et al. Pozzolanic evaluation of

mechanical-thermal composite activation of low-quality coal gangue and its impacts on the hydration properties of ordinary Portland cement. *Journal of Building Engineering*, **2025**, 113: 114237. https://doi.org/10.1016/j.jobe.2025.114237.

[8] Sui, S., He, G., Jiang, C., et al. Investigation on the activation of various coal gangues and the reaction mechanism with portlandite. *Construction and Building Materials*, **2025**, 463: 140120. https://doi.org/10.1016/j.conbuildmat.2025.140120.

[9] Qiu, J., Liu, Y., Li, L., et al. Study on frost resistance and deterioration law of manufactured sand coal gangue concrete. *Construction and Building Materials*, **2025**, 470: 140544. https://doi.org/10.1016/j.conbuildmat.2025.140544.

[10] Gao, S., Zhao, S., Yang, L., et al. Synergistic effects of fly ash-cement slurry and CO_2 mineralization on coal gangue aggregate and its concrete properties. *Construction and Building Materials*, **2025**, 465: 140225. https://doi.org/10.1016/j.conbuildmat.2025.140225.

[11] Wang, Y., Zhang, X., Su, L., et al. Study on the influence of composite modified coal gangue coarse aggregate on the mechanical properties of concrete and mesoscopic simulation. *Journal of Building Engineering*, **2025**, 106: 112549. https://doi.org/10.1016/j.jobe.2025.112549.

[12] Zhang, T., Zhu, Q., Shan, G. Mechanical properties of steel tubes filled with coal gangue concrete in a corrosive environment. *Alexandria Engineering Journal*, **2025**, 126: 418–440. https://doi.org/10.1016/j.aej.2025.04.076.

[13] Zhuang, Y., Deng, Q., Hou, M., et al. Clarifying the role of aggregate characteristics in the rheological and mechanical properties of coal gangue aggregate concrete with a packing perspective. *Journal of Building Engineering*, **2025**, 111: 113121. https://doi.org/10.1016/j.jobe.2025.113121.

[14] Kazmi, M. A., Meesaraganda, L. V. P. Enhancement of the performance of concrete and flexural behaviour of beam using two-step CO_2-mineralization. *Structures*, **2025**, 79: 109412. https://doi.org/10.1016/j.istruc.2025.109412.

[15] Cheng, X., Tian, W., Yuan, Q., et al. Response surface optimization of CO_2-mixing mineralization concrete: Balancing mechanical properties and carbon sequestration. *Construction and Building Materials*, **2025**, 471: 140648. https://doi.org/10.1016/j.conbuildmat.2025.140648.

[16] Hu, S., Liu, Q., Cai, H., et al. Performance of limestone calcined clay cement (LC3) made with CO_2-mineralized concrete slurry waste. *Journal of Cleaner Production*, **2024**, 472: 143476. https://doi.org/10.1016/j.jclepro.2024.143476.

[17] Zuo, W., Zhao, X., Luo, J., et al. Investigating the impact of carbonation curing concentrations on the mechanical properties and microstructure of recycled concrete. *Journal of Building Engineering*, **2024**, 96: 110465. https://doi.org/10.1016/j.jobe.2024.110465.

[18] Lin, X., Li, X., Liu, H., et al. A review on carbon storage *via* mineral carbonation: Bibliometric analysis, research advances, challenges, and perspectives. *Separation and Purification Technology*, **2024**, 338: 126558. https://doi.org/10.1016/j.seppur.2024.126558.

[19] Gu, X., Wang, S., Liu, J., et al. Improving physical properties, microstructure and actual carbon sequestration of steel slag based autoclaved aerated concrete by accelerated carbonation. *Journal of Building Engineering*, **2024**, 94: 110045. https://doi.org/10.1016/j.jobe.2024.110045.

[20] Lu, K., Jiang, B., Xiao, Y., et al. Study on inhibiting effects of melamine polyphosphate on pulverized coal explosion: Investigation from macro and micro perspectives. *Fuel*, **2024**, 360: 130574. https://doi.org/10.1016/j.fuel.2023.130574.

[21] Shao, Z., Cao, M. Hydration mechanism of limestone calcined clay cement containing calcined coal gangue. *Construction and Building Materials*, **2024**, 438: 136906. https://doi.org/10.1016/j.conbuildmat.2024.136906.

[22] Cardoso, J. V. S., Martins, A. J., Oliveira, A. C., et al. Structural and surface properties of oxides derived from layered double hydroxides (LDHs): Effects on the bioproducts obtained in the glycerol valorization. *Molecular Catalysis*, **2025**, 584: 115312. https://doi.org/10.1016/j.mcat.2025.115312.

[23] Santo, K. P., Neimark, A. V. Dissipative particle dynamics simulations in colloid and Interface science: A review. *Advances in Colloid and Interface Science*, **2021**, 298: 102545. https://doi.org/10.1016/j.cis.2021.102545.

[24] Chen, Q., Tian, J. A connection between the density and temperature of the Lennard-Jones fluids at equilibrium and the first peak of the radial distribution function. *Fluid Phase Equilibria*, **2023**, 567: 113709. https://doi.org/10.1016/j.fluid.2022.113709.

[25] Pereira, E., Pereira, E., Pianaro, S. A., et al. Combined effect of alkali-aggregate reaction (AAR) and internal sulfate attack (ISA): Microstructural and porous structure modifications of Portland cement mortars. *Construction and Building Materials*, **2023**, 362: 129676. https://doi.org/10.1016/j.conbuildmat.2022.129676.

[26] Kong, D., Wang, T., Zhang, J., et al. Improvement of strength and microstructure of low-carbon cementitious materials with high volume of calcined coal gangue. *Construction and Building Materials*, **2024**, 444: 137916. https://doi.org/10.1016/j.conbuildmat.2024.137916.

[27] Song, N., Huang, Y., Yang, G., et al. Incorporation of limestone calcined clay cement (LC3), seawater and sea-sand in ultra-high-performance engineered cementitious composites (UHPECC): Mechanical properties, hydration and microstructure. *Structures*, **2025**, 75: 108686. https://doi.org/10.1016/j.istruc.2025.108686.

[28] Sha, S., Ma, Y., Lei, L., et al. Effect of polycarboxylate superplasticizers on the growth of ettringite in deionized water and synthetic cement pore solution. *Construction and Building Materials*, **2022**, 341: 127602. https://doi.org/10.1016/j.conbuildmat.2022.127602.

[29] Hamada, H. M., Abed, F., Beddu, S., et al. Effect of Volcanic Ash and Natural Pozzolana on mechanical properties of sustainable cement concrete: A comprehensive review. *Case Studies in Construction Materials*, **2023**, 19: e02425. https://doi.org/10.1016/j.cscm.2023.e02425.

[30] Wang, B. J., Xie, Q., Sha, Y. T., et al. Research progress on the preparation of bamboo-based activated carbon for CO_2 adsorption. *New Carbon Materials*, **2025**, 40(2): 317–332. https://doi.org/10.1016/S1872-5805(25)60956-5.

[31] Genel, İ., Yardım, Y., Saka, C. Green synthesis of hierarchical nitrogen-doped porous activated carbon material based on biomass waste for high-performance energy storage as supercapacitor. *Biomass and Bioenergy*, **2025**, 197: 107818. https://doi.org/10.1016/j.biombioe.2025.107818.

[32] Yi, J., Fu, S., Huang, J., et al. Synergistic modification of recycled aggregate using carbonation and hydrophobic Nano-Silica: Effect on interfacial performance of recycled aggregate concrete. *Journal of Building Engineering*, **2025**, 107: 112740. https://doi.org/10.1016/j.jobe.2025.112740.

[33] Fan, J. Y., Lü, Z. G., Zhang, C. H., et al. Study on size effect of γ-Fe_2O_3 nanoparticles and gas atmosphere on carburization process. *Journal of Fuel Chemistry and Technology*, **2022**, 50(2): 218–226. https://doi.org/10.1016/S1872-5813(21)60157-3.

[34] Qin, L., Xie, Q., Bao, J., et al. Investigation of carbonation kinetics in carbonated cementitious materials by reactive molecular dynamics simulations. *ACS Sustainable Chemistry & Engineering*,

2024, 12(27): 10075−10088. https://doi.org/10.1021/acssuschemeng.3c07814.

[35] Mutisya, S. M., Kalinichev, A. G. Carbonation reaction mechanisms of portlandite predicted from enhanced *ab initio* molecular dynamics simulations. *Minerals*, **2021**, 11(5): 509. https://doi.org/10.3390/min11050509.

[36] Qin, L., Mao, X., Cui, Y., et al. New insights into the early stage nucleation of calcium carbonate gels by reactive molecular dynamics simulations. *The Journal of Chemical Physics*, **2022**, 157(23): 234501. https://doi.org/10.1063/5.0127240.

[37] Barbhuiya, S., Das, B. B. Molecular dynamics simulation in concrete research: A systematic review of techniques, models and future directions. *Journal of Building Engineering*, **2023**, 76: 107267. https://doi.org/10.1016/j.jobe.2023.107267.

[38] Wang, Y., Ivashko, A., Carstensen, B., et al. Acid-resistant zeolite RHO for deep dehydration. *Separation and Purification Technology*, **2023**, 325: 124661. https://doi.org/10.1016/j.seppur.2023.124661.

[39] Niu, J., Zhang, K. Molecular-scale insights into nanoconfined water-CO_2 interactions in geological carbon storage. *Chemical Engineering Science*, **2024**, 299: 120457. https://doi.org/10.1016/j.ces.2024.120457.

[40] Zhang, J., Peng, Y., Wang, C., et al. Interlayer water absorption expansion and surface hydration properties of montmorillonite and kaolinite. *Minerals Engineering*, **2025**, 234: 109713. https://doi.org/10.1016/j.mineng.2025.109713.

[41] Yang, L., Bao, L., Dong, T., et al. Adsorption properties of cellulose/guar gum/biochar composite hydrogel for Cu^{2+}, Co^{2+} and methylene blue. *International Journal of Biological Macromolecules*, **2023**, 242: 125021. https://doi.org/10.1016/j.ijbiomac.2023.125021.

Xuyang Zang is a Master's student at the School of Civil and Transportation Engineering, Hebei University of Technology. His research focuses on phase change materials for concrete and CO_2 curing of cementitious materials.

Lei Zhang received his PhD in Civil Engineering from the University of Western Ontario, Canada. He is currently a Yuanguang Scholar (Category B, Early Career Track) at Hebei University of Technology. His research interests include high-efficiency carbon capture using industrial solid waste, self-healing concrete, green and low-carbon concrete, machine-learning-enabled performance prediction of cementitious materials, paste backfill mining, and the resource utilization of industrial and mining solid waste. He has published more than 60 high-quality SCI papers in leading international journals such as *Renewable and Sustainable Energy Reviews*, *Cement and Concrete Research*, and *Composites Part B: Engineering*. His work has been cited more than 1700 times with an h-index of 23.

Moncef L. Nehdi is a Fellow of the Canadian Academy of Engineering, the Engineering Institute of Canada, the American Concrete Institute (ACI), the Canadian Society for Civil Engineering (CSCE), the Asia-Pacific Artificial Intelligence Association, and the International Artificial Intelligence Industry Alliance. He received numerous prestigious awards including the K.Y. Lo Medal of the Engineering Institute of Canada, the Sustainability Award from the American Concrete Institute, the Engineering Medal for Research and Development from Ontario Professional Engineers, the Ontario Premier's Research Excellence Award, ACI Award for Professional Achievement, CSCE Horst Liepholz Medal, CSCE Whitman Wright Award, Bill Curtin Medal from the United Kingdom's Institution of Civil Engineers, and Faculty Fellow Award for Excellence in Engineering Education from the American Society for Engineering Education. He served as Chair of the Materials and Mechanics Division of the Canadian Society for Civil Engineering, Deputy Chair of the RILEM Concrete Data Science Committee, Chair of the CSCE Cement and Concrete Committee, Chair of the American Concrete Institute (ACI) Recycled Materials Committee, and Section Chair of the Natural Science and Engineering Research Council of Canada (NSERC) Discovery Grant Committee 1509.

As a prolific author with over 500 peer-reviewed publications, he was listed among the world's most impactful civil engineers by Elsevier and the Shanghai Global Ranking of Academic Subjects and ranked in the Stanford University world's top 0.15% scientists. His research focuses on sustainable, eco-efficient and net-zero construction, civil infrastructure resilience, artificial intelligence and machine learning applications in civil engineering, innovative materials for construction and energy storage. He is also Canada's leader in civil engineering professional development programs offered to practicing engineers. His scholarly and scientific research was used in landmark construction projects in Canada and abroad, including the world's next-tallest building (Kingdom Tower), the world's fourth-tallest building (Abraj Al-Bait), the world's deepest and second-largest water treatment and pumping station (North Jeddah), the world's most venerated pedestrian bridge (Jamarat Bridge), Riyadh Financial District, and the NEOM Megacity project.